

Mechanically Asymmetrical Triboelectric Nanogenerator for Self-Powered Monitoring of In Vivo Microscale Weak Movement

Bolang Cheng, Jianxiu Ma, Gaoda Li, Suo Bai, Qi Xu, Xin Cui, Li Cheng, Yong Qin,* and Zhong Lin Wang*

Although much effort has been put in the studies of weak in vivo microscale movements due to its importance, the real-time, long-time, and accurate monitoring is still a great challenge because of the complexity of the in vivo environment. Here, a new type of mechanically asymmetrical triboelectric nanogenerator with ultrashort working distance and high anti-interference ability is developed to accurately and real-timely monitor the microscopically weak movement of intestinal motility at low frequencies even around 0.3 Hz. The intestinal status after the glucose absorption, and physiological states in different times also have been monitored successfully in the complex in vivo environment with many kinds of interference and noises. This work gives a new self-powered, long-time and in vivo technical way for the real-timely gastrointestinal motility monitoring, and contributes to the detection of every kind of gentle movements in various complex bio-systems.

1. Introduction

With the recent development of mobile electronics and internet of things, triboelectric nanogenerators (TENGs) based on the conjunction effect of contact electrification and electrostatic induction^[1] have attracted significant research efforts due to the potential advantages of low cost,^[2] high efficiency,^[3] simple structure,^[1] and diverse material options^[4,5] and the potential applications in robotics,^[6,7] human-computer interaction,^[8–10] especially in health-care.^[4,5,11–13] At low frequencies (<5 Hz), TENG can harvest irregular mechanical energy and convert it into large electrical output more efficiently compared to electromagnetic generators^[14] and possess the merits of no depolarization or heavy

metal pollution compared with piezoelectric nanogenerators by using situation adaptable and compatible materials.^[15–17] By now, TENGs have been widely used as energy harvesting devices,^[18–20] self-powered sensors,^[21–24] and provide a new possibility for movement monitoring due to their unique qualities and advantages.^[2,25,26] Especially, due to its unlimited mechanical power harvesting capacity, long working life, and adjustable size and biocompatibility, TENGs are expected to be one of the most promising self-powered mechanical sensors for in vivo mechanical movement monitoring,^[11,12,27,28] particularly for conversion of physiological signal to electrical signals, such as long-time in vivo monitoring of heart rate^[11,12] and breathing.^[27]

Besides the ordinary movement induced by the heartbeat and diaphragmatic movement, the weak in vivo microscale movements induced by smooth muscles (around 20 mN with frequency below 5 Hz^[29,30]), are quite important for the diagnosis, pathophysiological understanding, and the treatment of respirator, circulatory and digestive diseases, etc.^[31–34] For instances, increased airway smooth muscle contractility is the cardinal feature of asthma; contraction of vascular smooth muscles is directly related to pathological states of blood vessels, and it is responsible for stabilizing vessels and regulating blood flow and ensuring adequacy of local perfusion;^[34–36] the gastrointestinal motilities are of overriding importance to the obesity, constipation and indigestion in the digestive tract, deviant gastrointestinal smooth muscle contractility may be an important physiologic and pathophysiological mechanism.^[37–39] Conventionally, the weak

Dr. B. Cheng, Dr. G. Li, Dr. S. Bai, Dr. L. Cheng, Prof. Y. Qin
Institute of Nanoscience and Nanotechnology
School of Physical Science and Technology
Lanzhou University
Lanzhou 730000, China
E-mail: qinyong@lzu.edu.cn

Dr. J. Ma
Medical College
Northwest Minzu University
Lanzhou 730000, China

Dr. Q. Xu
School of Advanced Materials and Nanotechnology
Xidian University
Xi'an 710071, China

Dr. X. Cui
College of Chemistry and Chemical Engineering
Guangxi University
Nanning 530004, China

Prof. Z. L. Wang
College of Nanoscience and Technology
University of Chinese Academy of Sciences
Beijing 100049, China

Prof. Z. L. Wang
School of Material Science and Engineering
Georgia Institute of Technology
Atlanta, Georgia 30332, USA
E-mail: zhong.wang@mse.gatech.edu

 The ORCID identification number(s) for the author(s) of this article can be found under <https://doi.org/10.1002/aenm.202000827>.

DOI: 10.1002/aenm.202000827

in vivo microscale movements are often accompanied with the movement caused by other muscles^[16,37,40] and respiration.^[41] The interference from these background signals introduced by these movements makes the extraction and precise detection of microscale movements quite difficult. Despite the development of various sensing systems in recent decades, the analysis of in vivo smooth muscle motility such as bronchus,^[32] gallbladder,^[33] aorta,^[36] and small intestine^[37,42] are still challenging. For noninvasive methods like radiopaque markers, scintigraphy or wireless motility capsules, the precision and accuracy are not adequate (high scattering indexes cause low sensitivity $\approx 65\%–87\%$);^[30,43–48] while for invasive methods like manometry, tracheal and gastrointestinal obstruction is needed, which leads to the restriction of the sensing areas (the motility of segmental bronchus, jejunum and ileum is almost inaccessible)^[16,29,40,46,41,49–51] and makes the long-time, in situ monitoring of the in vivo smooth muscle motility unavailable.^[41,49] TENG has the potential to address the problem of real-time and long-time monitoring of weak microscale movements in vivo. However, limited by the strictly controlled encapsulation, size and thickness of TENG, useful signal is too easy to be flooded in the background artifacts. So, developing a real-time and long-time monitoring technique for detecting the weak in vivo microscale movements accurately is critically important.

Here, a new type of mechanically asymmetrical and ultrasensitive TENG (ATNG) with ultrashort working distance of only a few micrometers is designed and fabricated. It is further developed to realize a self-powered, long-time and accurately in vivo monitoring of the weak microscale muscle motility. And it has a high anti-interference capability when in the highly interferences in vivo environment. ATNG's mechanically asymmetrical structure avoids the interference from muscle movements, respiration and other intestinal peristalses during the duodenal motility monitoring process. After being implanted into the rabbit's abdominal cavity, the periodic contractions at a frequency of ≈ 0.32 Hz is precisely detected, and the peristalsis of the duodenum is monitored in real time for a long time. It is found that the intestinal peristalsis is accelerated by glucose absorption (frequency increases from 0.31 to 0.41 Hz within 5 min), and the long-time monitoring indicates different duodenal peristalsis states during different time periods and different physiological states.

2. Results and Discussion

The structure of ATNG is composed of inner and outer parts separated by a 20 μm air gap and each part has 4 layers: the friction material, electrode, substrate, and encapsulation material, as demonstrated in **Figure 1** and **Figure S1**, Supporting Information. **Figure 1** shows the SEM images of the cross section of ATNG. Such design of ATNG has a mechanically asymmetric structure (ultra-flexible inner part and relatively hard outer parts), which ensures its high adaptability to detect feeble forces and isolate interference from outside in the high-noise in vivo environment (as demonstrated in the right part of **Figure 1**); and a working distance as short as several micrometers which ensures its capability to precisely detect the microscopic movement of intestinal peristalses. Besides, the whole assembled

ATNG has an ultrathin structure (less than 100 μm thick) with a tiny area (1 cm \times 7 cm) and excellent flexibility, as shown in the insets of **Figure 1** and **Figure S2**, Supporting Information, which means it is suitable for most in vivo environment monitoring through implantation.

For the inner part, 20- μm -thick PDMS film (the Young's modulus is 750 kPa) with Cr/Ag electrode on one side is chosen to be the soft substrate to obtain a large deformation under feeble force. PDMS micro/nanopillars etched by Reactive Ion Etching (RIE) on the other side of the PDMS film act as electron attracting friction material, as shown in the middle part and the upper right corner of **Figure 1**. For the outer part, 30- μm -thick PET film (the Young's modulus is 4600 MPa) with Cr/Ag electrode on inner side is chosen to be the hard substrate, and polyamide-6 (PA-6) microbelts are electrospun on Cr/Ag electrode as electron losing friction material (the SEM image of PA-6 microbelts is shown in the middle and the lower right corner of **Figure 1**). PA-6 microbelts can reduce the thickness of friction layer while PDMS micro/nanopillars can increase the friction area, which ensure the largest open-circuit voltage of 40 V and short-circuit current of 0.5 μA for microscale weak movements, as shown in **Figures S3–S4**, Supporting Information) and long-time working ability of ATNG. Finally, the ATNG is encapsulated by PDMS to enhance the biocompatibility, robustness and stability in in vivo environment. The upper part of **Figure 1** illustrates the detailed working mechanism of ATNG, with a periodic change of working distance from I to III, and III to I, the amount of induced charges in Cr/Ag electrodes changes periodically, which produces an alternating current between electrodes. In this way, ATNG will have a large electrical output even the working distance is just 20 μm as the simulations demonstrated, where the largest potential difference can reach 360 V (bottom part of **Figure 1**).

Furthermore, the novel structure character including extremely small thickness and narrow air gap makes this ATNG has an ultrashort working distance and ability to harvest and detect the microscopic movement. Driven by the simulated intestinal peristalsis with microscopic movement provided by a linear motor, the open-circuit voltage and the short-circuit current of ATNG reaches 109 mV and 1.1 nA respectively under a 5- μm -amplitude perturbation, as shown in **Figure 2b** and **Video S1**, Supporting Information, which enable the accuracy to detect the gentle peristalsis of intestines. Additionally, when external triggering forces with different frequencies are applied on ATNG, the open-circuit voltage and short-circuit current output of ATNG (**Figure 2** and **Figure S5**, Supporting Information) show that the largest error between applied frequencies and corresponding measured frequencies is within 0.02 Hz, and the accuracy of detected frequencies is around 99.3%, extremely in intestinal peristalses frequency (0.3–0.5 Hz), as shown in **Figure 2** and **Figures S6** and **S7**, Supporting Information.

Due to the significant difference in Young's modulus of soft and hard substrates, the deformation and electrical output of ATNG would be distinctly different when the force is applied from different directions and onto different substrates. To better understand the relationship between electrical output and the mechanically asymmetrical structure of ATNG, the deformation and electrical output are simulated by finite

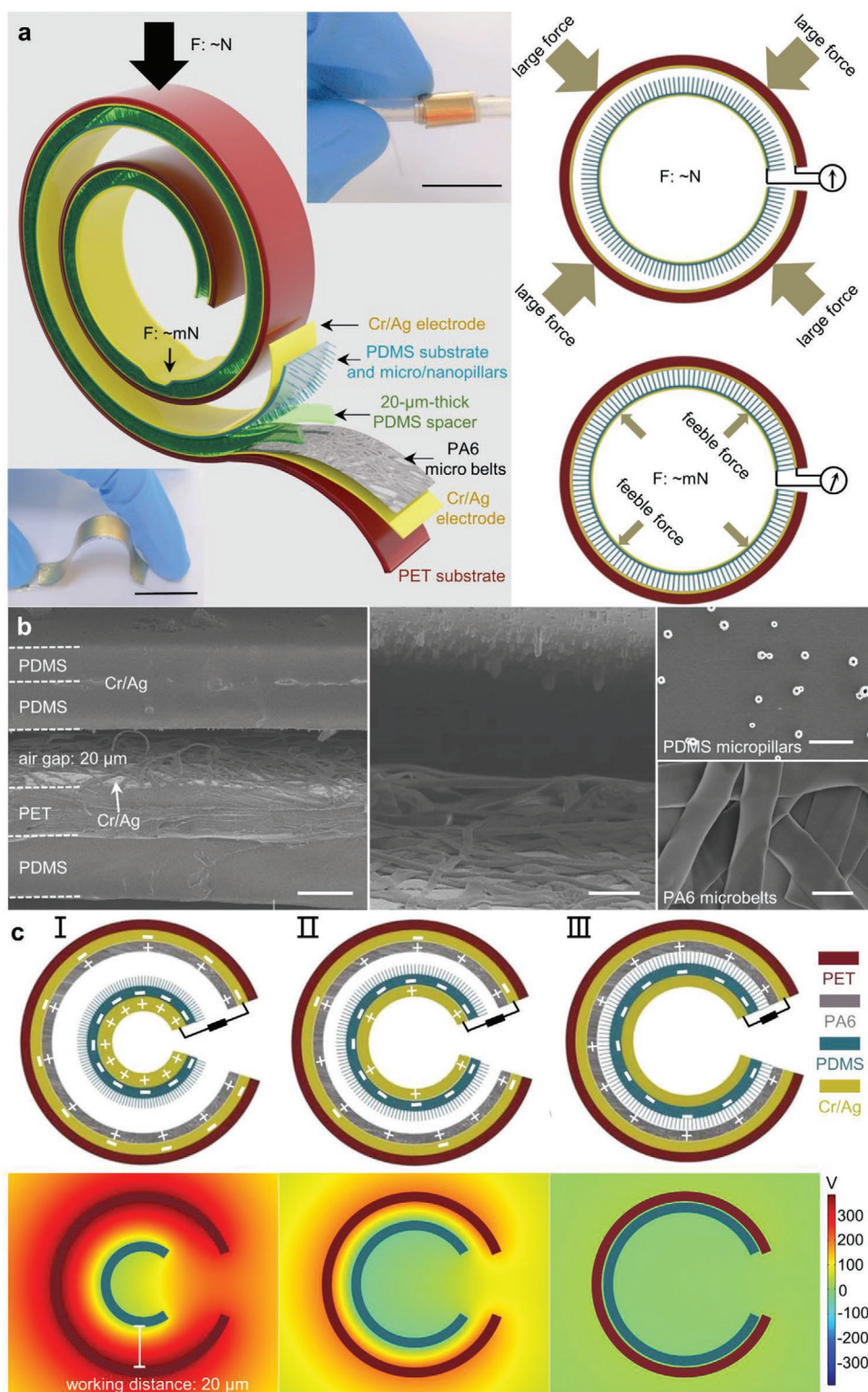


Figure 1. Schematic diagram, structure and working mechanism of the ATNG. a) The device structure of the ATNG. A 20- μ m-thick PDMS spacer is used to ensure an ultrashort working distance (20 μ m). The inset photos show an actual image of the ATNG (scale bar represents 1 cm). b) Scanning electronic microscopy (SEM) images of the ATNG. The left part is the cross section of the ATNG. The middle part is the internal friction layers of the ATNG composed of PDMS micro/nanopillars and PA-6 microbelts. The right part is the top views of PDMS micro/nanopillars and PA6 microbelts. Scale bars in the left, middle, top right, and bottom right parts of figure (b) represent 20, 5, 2, and 2 μ m respectively. c) Schematic of the processes of charge transferring (top part) and simulated potential distribution (bottom part) in different working state of the ATNG.

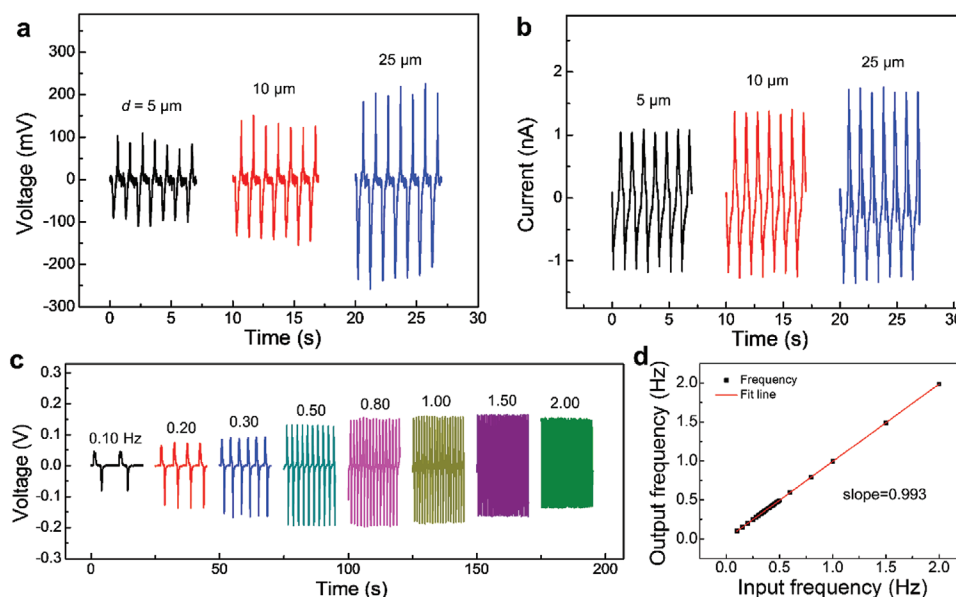


Figure 2. The accurate response for driving distance and frequency of ATNG. a) The open-circuit voltage and b) short-circuit current output of the ATNG under different micro driving distances. c) The open-circuit voltage output of the ATNG under periodically driving sinusoidal forces with different frequencies. d) The correspondence relation between the frequency of open-circuit voltage output and that of input driving force, where slope = 0.993 illustrates the accuracy of frequency detecting (deviation: $\approx \pm 0.7\%$).

element calculations using COMSOL software. When the pressure ranging from 0.1 to 1 Pa is applied onto the PDMS soft substrate, the deformation of the ATNG varies from 0.48 to 4.75 μm and the corresponding capacitance change ΔC_{max} is 26.78 pF, in contrast with the 743 to 74.28 pm deformation and

negligible capacitance change of 0.32 fF when the same weak pressure is applied onto the PET hard substrate, as shown in **Figure 3** and **Figure S8**, Supporting Information. As the output of a TENG is highly related to the capacitance change,^[52] the remarkable variations of capacitance change caused by the

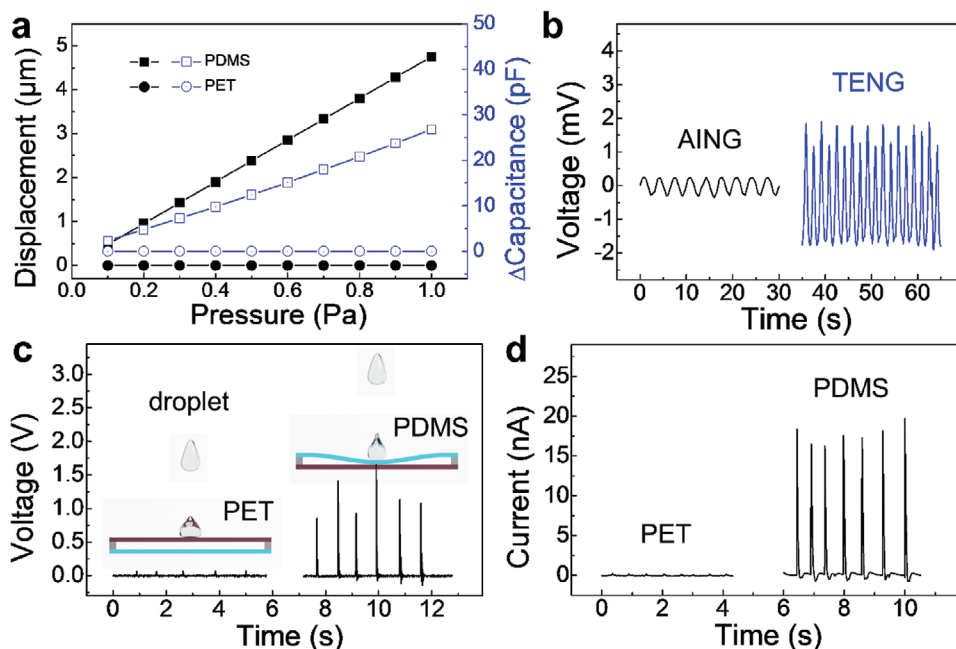


Figure 3. The mechanical asymmetry and output asymmetry of the ATNG. a) Simulated deformations and capacitance change of ATNG with small pressure exerted on the PDMS side, and PET side, respectively. b) Simulated output voltage of the ATNG (PDMS-PET) and a conventional symmetric TENG (PDMS-PDMS) driving by the simultaneous simulated peristalsis (28 Pa and 0.3 Hz) on one side and the simulated respiration (200 Pa and 0.6 Hz) on the other side. c) The open-circuit voltage and d) short-circuit current of the ATNG driven by a water droplet from the PET side and PDMS side, experimentally.

asymmetric structure of the ATNG is utilized to eliminate the interference from respiration during the GI monitoring.

To further confirm the ATNG's performance of harvesting and detecting the weak movement and its anti-interference ability, a simulation was carried out. Sinusoidal forces are applied normally onto both substrate sides: simulated pressure of GI peristalsis (28 Pa at 0.3 Hz) is applied onto the PDMS soft substrate and simulated pressure of respiration (200 Pa at 0.6 Hz) is applied onto the PET hard substrate of ATNG. The electrical output of ATNG is shown in the left part of Figure 3: the sinusoidal output signal has a frequency of 0.3 Hz and amplitude of 0.3 mV, indicating the complete elimination of interference. When only the simulated pressure of respiration is applied, the electrical output of ATNG is also negligible (amplitude around 150 nV as shown in Figure S9, Supporting Information). To give a clearer illustration of the importance of mechanical asymmetry of ATNG, the same pressures are applied onto the conventional symmetrical TENG with double PDMS substrate (its detailed fabrication process is given in Experiment Section) under the same conditions. The output signal is composed by two superimposed sinusoidal signals with frequencies of 0.6 Hz and 0.3 Hz, as shown in the right part of Figure 3. In addition, the sensitivity of ATNG to feeble forces and its anti-interference ability are also verified through a water drop experiment. The water droplet (≈ 31 mg) is dropped on the soft PDMS and hard PET sides respectively from 10 cm height above the ATNG. The open-circuit voltage (Figure 3) and short-circuit current (Figure 3) of ATNG when water drops on PDMS side are around 1.0 V and 20 nA respectively, while those signals when water drops on PET side are negligible, which means the ATNG has the ability to eliminate the external interference from the direction of hard PET substrate. Moreover, the sensitivity and the detectable limit of ATNG toward the weak force can reach $0.67 \text{ nA (mN)}^{-1}$ and 3.04 mN, respectively (Figure S10, Supporting Information).

In order to in vivo monitor the peristalsis of the duodenum, ATNG is implanted into the abdominal cavity of the rabbit, as shown in Figure 4. Since the contraction of duodenal peristalsis is quite gentle ($F \approx 20$ mN) and slow ($f \approx 0.3$ Hz),^[28,29] it is almost unobservable and overwhelmed by the movement of respiration or blood vessel, as demonstrated by the Videos S2 and S3, Supporting Information. When a conventionally symmetrical TENG is implanted into the same position of rabbit,

the monitored electrical signal is different with the form of duodenal peristalsis but rather close to the form of respiration as shown in Figure S11, Supporting Information, since the force and the distance of duodenal peristalsis are much smaller than and obscured by that of breath. When the ATNG is implanted into the abdominal cavity, where the soft PDMS substrate is attached onto the duodenum and hard PET substrate is faced to other intestines and abdominal cavity, the signals of duodenal peristalsis are detected as shown in Figure 4. The electrical output caused by duodenal peristalsis is quite lower than that caused by respiration (less than 0.2 mV compared with 1 mV), and the frequency of the former is smaller than respiration. This is clearer in the domain field (Figure 4) after doing a fast Fourier transformation of the electrical signals: the electrical signal monitored by ATNG is dominated by the frequency at 0.32 Hz, while that monitored by conventional TENG is dominated by the frequency at 0.58 Hz. These measured frequencies by ATNG and conventional TENG are in consistent with the previous reports of the frequencies of duodenal peristalsis and breath of rabbits respectively, which indicates that the interference of respiration is eliminated successfully by mechanically asymmetrical structure design of ATNG.

After interference signals have been excluded to ensure the signal's trustworthiness, a real-time duodenal peristalsis monitoring by the ATNG is demonstrated. The duodenal peristalsis under anesthesia in the fasting state is monitored as shown in Figure 5, and the electrical signals of 5 and 10 min after intragastric administration with glucose solution (5 mL, 5 wt%) are shown in Figure 5c. The respective frequencies of duodenal peristalsis with 0.31 Hz, 0.41 and 0.33 Hz are observed in different physiological states, which could manifest that the peristalsis of duodenum becomes violent at first and then gradually decelerates after intragastric administration upon direct stimulation by the glucose solution. It is consistent with the past reported physiological activity of rabbit in different physiological states.^[44,53] From above results, it can be seen that this ATNG has the ability to monitor and distinguish the different physiological states of duodenal peristalsis. Subsequently, a long-time monitoring of duodenum without anesthesia is carried out, and the peristalsis on the fifth day after implantation is analyzed. The signals of rabbit's duodenal peristalsis from 01:00 am to 10:00 am can be divided into 3 phases during this time period. Taken from differently characteristic time periods

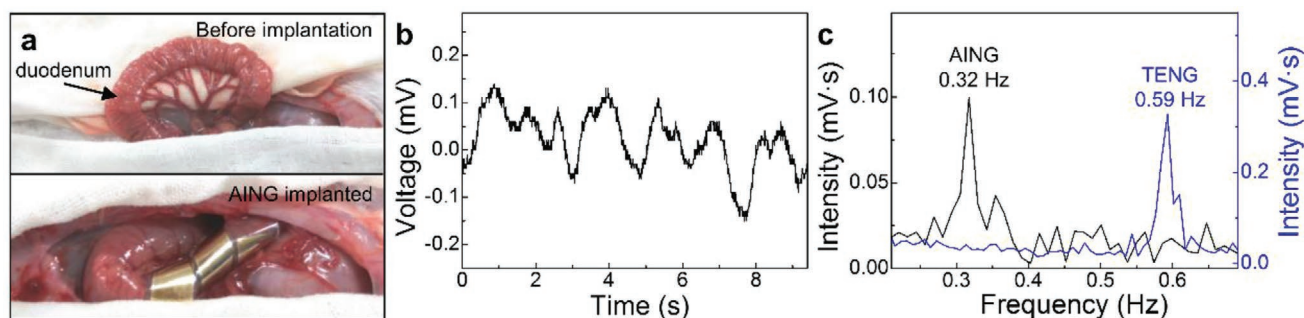


Figure 4. In vivo duodenal peristalsis monitoring by ATNG. a) Optical image of the ATNG implanted in rabbit's cavity. b) The open-circuit voltage signals of the rabbit's duodenal peristalsis monitored by the ATNG. c) The spectrum of signals obtained by a fast Fourier transformation of the time domain output voltage monitored by the ATNG and a conventional symmetric TENG.

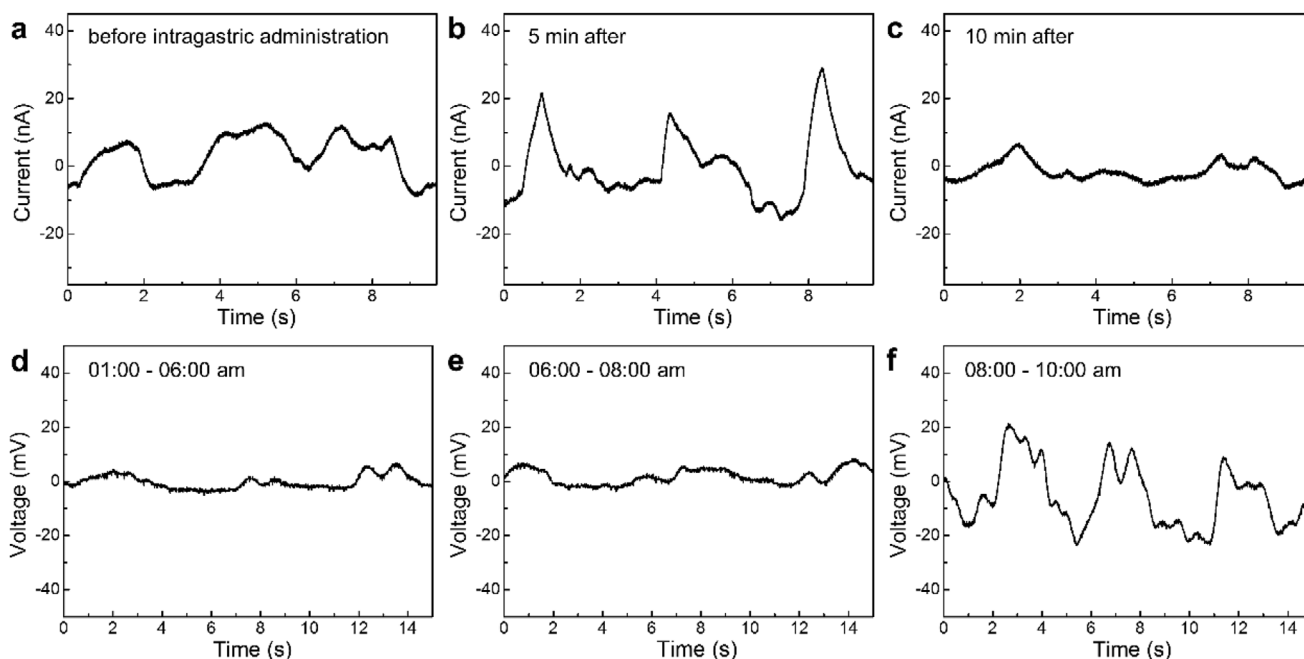


Figure 5. The real-time and long-time monitoring of duodenal peristalsis by the ATNG. The current signals monitored by ATNG under duodenal peristalsis status a) before, b) 5 min after, and c) 10 min after intragastric administration with 5 wt% glucose solution. Long-time monitoring of duodenal peristalsis state using ATNG during different time periods on the fifth day after implantation: d) during 01:00–06:00 am, e) during 06:00–08:00 am, and f) during 08:00–10:00 am.

respectively, the characteristically electrical signals in Figure 5f show different wave structures and amplitudes (5, 10, and 20 mV respectively) and indicate the variation of duodenal peristalsis. During 01:00–06:00 am, the duodenal peristalsis is gentle and slow since the rabbit is not vibrant at night. After 06:00 am, the rabbit is woken by researchers, resulting in the gradually violent peristalsis of duodenum with larger amplitude and higher frequency, which is in accordance with the previous report about the difference of peristalsis of intestine in different times.^[54] Later, the rabbit is fed with fresh grass and clear water at 08:00 am and the electrical output shows the largest amplitude and highest frequency. Furthermore, even after 5 days continuous working, the high sensitivity to feeble forces of ATNG is preserved: ATNG exhibits steady and comparable open-circuit voltage and short-circuit current (Figure S12, Supporting Information). This is also confirmed by the SEM images (Figure S13, Supporting Information) of the friction layers after 5 days continuous working: no obvious deterioration of the PA-6 microbelts or PDMS micro/nanopillars is observed in comparison with that before implantation (Figure 2). All these performances clearly prove the capability of ATNG for the self-performed in vivo and long-time monitoring of the intestinal motility in living animals, as well as its capability for the probable monitoring of other slight movements in other complex systems.

3. Conclusion

In summary, a novel TENG with mechanically asymmetrical structure is designed and fabricated to realize the self-powered

and real-timely in vivo monitoring of the weak smooth muscle motility with the elimination of interference from muscle movement and respiration. As verified by the finite element simulation, water droplets, micro distances and frequencies contrast experiments, this ATNG exhibits high sensitivity to micro distances (the open-circuit voltage and the short-circuit current of ATNG reaches 109 mV and 1.1 nA respectively under a 5- μ m-amplitude perturbation) and low frequencies (the deviation of detected frequencies is around $\pm 0.7\%$) and has the excellent anti-interference ability. Implanted into the rabbit's abdominal cavity, the peristalsis of duodenum is monitored by this ATNG: contracting at frequency around 0.32 Hz, the duodenal peristalsis is accelerated after glucose absorption and shows different peristalsis states during different time periods and physiological states. In conclusion, this ATNG has the great potential for the accurate monitoring of weak movement in various complex systems with diverse components and multifarious mutually interfered slight movements, especially bio-systems.

4. Experimental Section

Materials and Chemicals: PET films were used for the fabrication of ATNG. PDMS (DOWSIL) was used for the fabrication of the substrate and the electron attracting friction material. PA6 (Sinopharm Chemical Reagent Co., Ltd) was used for the fabrication of the electron losing friction material. Polyvinylpyrrolidone (PVP) (Alfa Aesar Co., Inc.) was used for the fabrication of the acrifical layers. Absolute ethanol (>99%, Lian longbohua (Tianjin) Pharmaceutical Chemistry Co., Ltd) and deionized (DI) were used for dissolving the PVP sacrificial layers and cleaning substrate and device.

Preparation of PVP Solution and PA-6 Solutions: The PVP solution was prepared by mixing and stirring 10 wt% PVP and 90 wt% ethanol in

water bath at 60 °C for 12 h to make PVP completely dissolved. The PA-6 solution was prepared by mixing and stirring 22.7 wt% PA-6, 31.8 wt% dichloromethane and 45.5 wt% formic acid in water bath at 60 °C for 1 h to make PA-6 completely dissolved. All reagents were analytically pure and used without any further purification.

Fabrication of the TENG with PDMS-PDMS Mechanically Symmetrical Structure: The fabrication of the TENG with PDMS-PDMS mechanically symmetrical structure was based on the design of a fully packaged structure and different friction layers with the same material (PDMS) substrate. First, two pieces of clean 100- μm -thick PET films were cut into 1.2 cm \times 8 cm. Second, the PVP solution was coated on one side of the PET films and dried at 60 °C for 30 min to form 5- μm -thick PVP sacrificial layers. Then, the pre-mixed PDMS elastomer and curing agent was coated on PVP sacrificial layers and solidified at 80 °C for 30 min to form the 20- μm -thick PDMS films. Then, the Cr/Ag electrodes with the size of 0.8 cm \times 6.8 cm were sputtered by the magnetron sputtering on PDMS films, and the copper wires were contacted to the Cr/Ag electrodes as the electrical signals acquisition ports. After that, two pieces of pre-prepared films were separated as part I and part II to be treated differently. The pre-mixed PDMS elastomer and curing agent was coated on the Cr/Ag electrode of part I and solidified at 80 °C for 2 h to form a 20- μm -thick PDMS friction layer. Then, the PDMS friction layer was placed into the Reactive Ion Etching chamber, the pressure in the chamber was evacuated to a base pressure of 3×10^{-4} Pa, the Ar, O₂, and CF₄ were introduced at a flow rate of 11, 10, and 71 sccm, respectively, the glow discharge was ignited at 250 W in a working pressure of 5 Pa for 1 h. The PA-6 microbelts friction layer were fabricated on the Cr/Ag electrode of part II by electrospinning PA-6 solution for 5 min with the voltage of 18 kV, propulsion velocity of 1 mL h⁻¹ and the distance between the needle and the film of 18 cm. Then, the pre-mixed PDMS elastomer and curing agent was coated on the edge of PDMS friction layer of part I, the friction layer of part II was adhered on the friction layer of part I face to face by the liquid PDMS and solidified at 80 °C for 2 h to form a 20- μm -thick, 1-mm-wide PDMS spacer, then the friction layer-air-friction layer sandwich structure was fabricated. Finally, the sandwich structured TENG was soaked in ethanol for 12 h in room temperature, and the TENG with PDMS-PDMS mechanically symmetrical structure detaches from two 100- μm -thick PET films by dissolving the PVP sacrificial layers. And the TENG with PDMS-PDMS mechanically symmetrical structure was acquired.

Fabrication of the ATNG with PET-PDMS Mechanically Asymmetrical Structure: As Figure S1, Supporting Information shows, compared with the fabrication of the TENG with PDMS-PDMS mechanically symmetrical structure, the ATNG with PET-PDMS mechanically asymmetrical structure was designed by replacing the 20- μm -thick PDMS film of the PDMS-PDMS mechanically symmetrical structure TENG with 30- μm -thick PET film as substrate of the PA-6 microbelts, and leave all other materials and processes unchanged. First, the part I of ATNG with PET-PDMS mechanically asymmetrical structure was the same as the part I of TENG with PDMS-PDMS mechanically symmetrical structure. Second, one pieces of clean 30- μm -thick PET film with a size of 1.2 cm \times 8 cm was used as the substrate of part II of ATNG. The pre-mixed PDMS elastomer and curing agent was coated on one side of PET and solidified at 80 °C for 30 min to form the 20- μm -thick PDMS encapsulation layer. Then, the Cr/Ag electrodes with the size of 0.8 cm \times 6.8 cm were sputtered by the magnetron sputtering on another side of PET films, and the copper wires were contacted to the Cr/Ag electrodes as the electrical signals acquisition ports. The PA-6 microbelts friction layer were fabricated on the Cr/Ag electrode of part II by electrospinning PA-6 solution for 5 min with the voltage of 18 kV, propulsion velocity of 1 mL h⁻¹ and the distance between the needle and the film of 18 cm. Then, the pre-mixed PDMS elastomer and curing agent was coated on the edge of PDMS friction layer of part I, and the friction layer of part II was adhered on the friction layer of part I face to face by the liquid PDMS and solidified at 80 °C for 2 h to build a 20- μm -thick, 1-mm-wide PDMS spacer, then the friction layer-air-friction layer sandwich structure was fabricated. Finally, the sandwich structured ATNG was soaked in ethanol for 12 h in room temperature, and the ATNG with PET-PDMS

mechanically asymmetrical structure detaches from the 100- μm -thick PET film by dissolving the PVP sacrificial layer. The ATNG with PET-PDMS mechanically asymmetrical structure was acquired.

Simulation: The finite element calculations of deformation and electrical output were carried out by COMSOL software. In the calculation, the thicknesses of PET and PDMS films were set as 30 and 20 μm , the widths of the device were set as 1000 μm , and the dielectric constants of PET and PDMS films were set as 3.6 and 2.75, the Young's modulus of the PET and PDMS films were set as 4600 and 750 kPa, the charge densities in PET and PDMS surface were set as $\pm 11.2 \mu\text{C m}^{-2}$ (obtained by the time integral of largest short-circuit current of ATNG in Figure S3, Supporting Information), and the gap between the PET and PDMS varies from 20 to 0 μm . When the force applied on the soft substrate side, the deformation and output open-circuit voltage of ATNG were 50 000 times and 64 000 times larger than that of ATNG when the force applied on its hard substrate side, which was due to the huge Young's modulus difference of different substrates. Both of them illustrate that the hard substrate of ATNG can be used to effectively eliminate the influences of interference.

Water Droplets Experiment: First, the dropper with deionized water inside was fixed on an iron platform, and the distance between the dropper and the desktop was set as 10 cm. Second, the ATNG was put on the desktop and its soft or hard substrate faces to the dropper. Then, the open-circuit voltage and short-circuit current output of ATNG was recorded by the test instrument when the water droplets fall from the dropper slowly to the soft substrate of ATNG drop by drop.

ATNG Implantation and Experiments In Vivo: All the animals and experimental works were processed according to the ethical review guidelines of Northwest Minzu University and in compliance with Chinese law. The Lanzhou Institute of Biological Products provides adult New Zealand Rabbits of 2–2.5 kg body weights. All the animals were housed in polypropylene cages with free access to standard laboratory animal diet and clean water, animals were checked daily for health and husbandry conditions during the whole feeding stage. Temperature was set at 21 ± 5 °C and relative humidity at $50 \pm 10\%$ with normal light-dark cycle. First, the rabbits were fasted for 24 h with clean water fed only. Second, the rabbits re anesthetized with urethane (dose 50 mg kg⁻¹) by intravenous injecting into the veins of ear. Then, the rabbits were fixed on the fixture and the hairs of the abdomen were removed. Then, an incision of about 8 cm in length was made in the middle of the abdomen. Simultaneously, the aseptic gauzes were placed on both sides of the incision and fixed with forceps to prevent bacterial infection. After laparotomy, the surgical field was exposed. Then, the small intestine and the greater omentum were pushed to the medial side of the abdominal cavity, and the duodenum was founded and taken out from the abdominal cavity carefully. Then, the surrounding area of duodenum was covered with aseptic gauzes which were soaked in physiological saline previously to protect other tissue. After that, the TENG with PDMS-PDMS mechanically symmetrically structure passes through the mesentery and blood vessels were avoided carefully. After that, the TENG was wrapped around the surface of duodenum and the ends of the TENG were sutured to the surface of duodenum to prevent shedding. Then, the duodenum was placed back to abdominal cavity and the electrical output of the TENG were recorded. After that, the duodenum was taken out from abdominal cavity again and this TENG was replaced by ATNG with PET-PDMS mechanically asymmetrically structure for duodenal peristalsis monitoring. Here, the implantation methods were consistent with the steps above, but the soft substrate of ATNG was faced to duodenum and the hard substrate of ATNG was faced to other intestines for eliminating the effects of interference. Then, the duodenum was placed back to abdominal cavity and the electrical output of the ATNG were recorded again. Finally, the incision was sutured and disinfected abide by the basic principle of clinical, here, the ATNG with PET-PDMS mechanically asymmetrically structure was stay in abdominal cavity but the ends of copper wires were in vitro.

Measurement and Characterization: The ultrashort distance was applied by a liner motor (K15-W/C-2, LinMot). A Model SR560 (Stanford Research Systems) low noise voltage preamplifier was used to measure

the open-circuit voltage, while a SR570 low-noise current amplifier (Stanford Research Systems) was used to measure the short-circuit current.

Supporting Information

Supporting Information is available from the Wiley Online Library or from the author.

Acknowledgements

B.C., J.M., and G.L. contributed equally to this work. This research was supported by the support from Joint fund of Equipment pre-Research and Ministry of Education (NO. 6141A02022518), the National Program for Support of Top-notch Young Professionals, the Fundamental Research Funds for the Central Universities (No. lzujbky-2018-ot04), NSFC (NO. 81702095, 81801847). The authors also thank Dr. Xiaofeng Jia, Shaoshuai Niu, Yaqin Ding, Leixin Meng, Ruichao Zhang for helpful discussions and assistance in experiments.

Conflict of Interest

The authors declare no conflict of interest.

Keywords

gastrointestinal motility monitoring, implantable sensors, self-powered nanodevices, triboelectric nanogenerators, weak movement detection

Received: March 3, 2020

Revised: April 30, 2020

Published online: May 28, 2020

- [1] F. R. Fan, Z. Q. Tian, Z. L. Wang, *Nano Energy* **2012**, *1*, 328.
- [2] F. R. Fan, L. Lin, G. Zhu, W. Wu, R. Zhang, Z. L. Wang, *Nano Lett.* **2012**, *12*, 3109.
- [3] Y. Xie, S. Wang, S. Niu, L. Lin, Q. Jing, J. Yang, Z. Wu, Z. L. Wang, *Adv. Mater.* **2014**, *26*, 6599.
- [4] P. Song, S. Kuang, N. Panvar, G. Yang, D. J. H. Tng, S. C. Tjin, W. J. Ng, M. B. A. Majid, G. Zhu, K. Yong, Z. L. Wang, *Adv. Mater.* **2017**, *29*, 1605668.
- [5] Q. Zheng, B. Shi, Z. Li, Z. L. Wang, *Adv. Sci.* **2017**, *4*, 1700029.
- [6] Z. L. Wang, *ACS Nano* **2013**, *7*, 9533.
- [7] K. Dong, Z. Wu, J. Deng, A. C. Wang, H. Zou, C. Chen, D. Hu, B. Gu, B. Sun, Z. L. Wang, *Adv. Mater.* **2018**, *30*, 1804944.
- [8] Y. Yang, H. Zhang, Y. S. Zhou, Q. Jing, Y. Su, J. Yang, J. Chen, C. Hu, Z. L. Wang, *ACS Nano* **2013**, *7*, 9213.
- [9] T. Zhong, M. Zhang, Y. Fu, Y. Han, H. Guan, H. He, T. Zhao, L. Xing, X. Xue, Y. Zhang, Y. Zhan, *Nano Energy* **2019**, *63*, 103884.
- [10] Y. Dai, Y. Fu, H. Zeng, L. Xing, Y. Zhang, Y. Zhan, X. Xue, *Adv. Funct. Mater.* **2018**, *28*, 1800275.
- [11] Y. Ma, Q. Zheng, Y. Liu, B. Shi, X. Xue, W. Ji, Z. Liu, Y. Jin, Y. Zou, Z. An, W. Zhang, X. Wang, W. Jiang, Z. Xu, Z. L. Wang, Z. Li, H. Zhang, *Nano Lett.* **2016**, *16*, 6042.
- [12] Q. Zheng, H. Zhang, B. Shi, X. Xue, Z. Liu, Y. Jin, Y. Ma, Y. Zou, X. Wang, Z. An, W. Tang, W. Zhang, F. Yang, Y. Liu, X. Lang, Z. Xu, Z. Li, Z. L. Wang, *ACS Nano* **2016**, *10*, 6510.
- [13] H. Zhang, Y. Yang, T. Hou, Y. Su, C. Hu, Z. L. Wang, *Nano Energy* **2013**, *2*, 1019.
- [14] Y. Zi, H. Guo, Z. Wen, M. Yeh, C. Hu, Z. L. Wang, *ACS Nano* **2016**, *10*, 4797.
- [15] L. Gu, N. Cui, L. Cheng, Q. Xu, S. Bai, M. Yuan, W. Wu, J. Liu, Y. Zhao, F. Ma, Y. Qin, Z. L. Wang, *Nano Lett.* **2013**, *13*, 91.
- [16] C. Dagdeviren, F. Javid, P. Joe, T. V. Erlach, T. Bensele, Z. Wei, S. Saxton, C. Cleveland, L. Booth, S. McDonnell, J. Collins, A. Hayward, R. Langer, G. Traverso, *Nat. Biomed. Eng.* **2017**, *1*, 807.
- [17] J. H. Zhang, Y. Li, J. Du, X. Hao, Q. Wang, *Nano Energy* **2019**, *61*, 486.
- [18] L. Cheng, Q. Xu, Y. Zheng, X. Jia, Y. Qin, *Nat. Commun.* **2018**, *9*, 3773.
- [19] J. Liu, N. Cui, L. Gu, X. Chen, S. Bai, Y. Zheng, C. Hu, Y. Qin, *Nanoscale* **2016**, *8*, 4938.
- [20] J. H. Zhang, Y. Li, J. Du, X. Hao, H. Huang, *J. Mater. Chem. A* **2019**, *7*, 11724.
- [21] Y. Chen, Y. Wang, Y. Zhang, H. Zou, Z. Lin, G. Zhang, C. Zou, Z. L. Wang, *Adv. Energy Mater.* **2018**, *8*, 1802159.
- [22] L. Cheng, Y. Zheng, Q. Xu, Y. Qin, *Adv. Opt. Mater.* **2017**, *5*, 1600623.
- [23] H. Guan, D. Lv, T. Zhong, Y. Dai, L. Xing, X. Xue, Y. Zhang, Y. Zhan, *Nano Energy* **2020**, *67*, 104182.
- [24] Y. Fu, M. Zhang, Y. Dai, H. Zeng, C. Sun, Y. Han, L. Xing, S. Wang, X. Xue, Y. Zhan, Y. Zhang, *Nano Energy* **2018**, *44*, 43.
- [25] S. Wang, L. Lin, Z. L. Wang, *Nano Energy* **2015**, *11*, 436.
- [26] J. Bae, J. Lee, S. Kim, J. Ha, B. Lee, Y. Park, C. Choong, J. Kim, Z. L. Wang, H. Kim, J. Park, U. Chung, *Nat. Commun.* **2014**, *5*, 4929.
- [27] Q. Zheng, B. Shi, F. Fan, X. Wang, L. Yan, W. Yuan, S. Wang, H. Liu, Z. Li, Z. L. Wang, *Adv. Mater.* **2014**, *26*, 5851.
- [28] Z. L. Wang, G. Zhu, Y. Yang, S. Wang, C. Pan, *Mater. Today* **2012**, *15*, 532.
- [29] H. Elbrond, L. Ostergaard, B. Huniche, L. S. Larsen, M. B. Andersen, *Scand. J. Gastroenterol.* **1994**, *29*, 537.
- [30] R. C. Small, A. H. Weston, *J. Pharm. Pharmacol.* **1971**, *23*, 280.
- [31] N. J. Talley, T. Goodsall, M. Potter, *Aust. Prescr.* **2017**, *40*, 209.
- [32] K. Larsson, *Clin. Respir. J.* **2010**, *4*, 35.
- [33] B. Lavoie, B. Nausch, E. A. Zane, M. R. Leonard, O. B. Balemba, A. C. Bartoo, R. Wilcox, M. T. Nelson, M. C. Carey, G. M. Mawe, *Neurogastroenterol. Motil.* **2012**, *24*, e313.
- [34] K. H. Kuo, J. M. Leo, *Anat. Rec.* **2019**, *302*, 186.
- [35] O. V. Halaidych, C. L. Mummery, V. V. Orlova, *Biochem. Biophys. Res. Commun.* **2019**, *513*, 112.
- [36] A. J. A. Leloup, C. E. V. Hove, S. D. Moudt, G. R. Y. D. Meyer, G. W. D. Keulenaer, P. Fransen, *Physiol. Rep.* **2019**, *7*, e13934.
- [37] L. K. Cheng, G. Farrugia, *New Advances in Gastrointestinal Motility Research*, Springer, Dordrecht, Netherlands **2013**.
- [38] J. Keller, G. Bassotti, J. Clarke, P. Dinning, M. Fox, M. Grover, P. M. Hellström, M. Ke, P. Layer, C. Malagelada, H. P. Parkman, S. M. Scott, J. Tack, M. Simren, H. Törnblom, M. Camilleri, *Nat. Rev. Gastroenterol. Hepatol.* **2018**, *15*, 291.
- [39] M. Simren, J. Tack, *Nat. Rev. Gastroenterol. Hepatol.* **2018**, *15*, 589.
- [40] D. R. Merritt, F. Weinhaus, *Am. J. Phys.* **1978**, *46*, 976.
- [41] L. Yu, B. J. Kim, E. Meng, *Sensors* **2014**, *14*, 20620.
- [42] M. Camilleri, A. E. Bharucha, C. D. Lorenzo, W. L. Hasler, C. M. Prather, S. S. Rao, A. Wald, *Neurogastroenterol. Motil.* **2008**, *20*, 1269.
- [43] A. C. G. Van Baar, M. Nieuwdorp, F. Holleman, *Gastroenterology* **2018**, *154*, 773.
- [44] J. Schirra, M. Nicolaus, R. Roggel, M. Katschinski, M. Storr, H. J. Woerle, B. Göke, *Gut* **2006**, *55*, 243.
- [45] H. Deflers, F. Gandar, G. Bolen, F. Farnir, D. Marlier, *Vet. Anaesth. Analg.* **2018**, *45*, 510.
- [46] B. Hens, Y. Tsume, M. Bermejo, P. Paixao, M. J. Koenigsnecht, J. R. Baker, W. L. Hasler, R. Lionberger, J. Fan, J. Dickens, K. Shedden, B. Wen, J. Wsocki, R. Loebenberg, A. Lee, A. Frances, G. Amidon, A. Yu, G. Benninghoff, N. Salehi, A. Talatoff, D. Sun, G. L. Amidon, *Mol. Pharmaceutics* **2017**, *14*, 4281.
- [47] P. A. Muller, B. Koscsó, G. M. Rajani, K. Stevanovic, M. Berres, D. Hashimoto, A. Mortha, M. Leboeuf, X. Li, D. Mucida, E. R. Stanley, S. Dahan, K. G. Margolis, M. D. Gershon, M. Merad, M. Bogunovic, *Cell* **2014**, *158*, 300.
- [48] L. Grasa, E. Rebollar, M. Arruebo, M. Plaza, M. Murillo, *J. Physiol. Pharmacol.* **2004**, *56*, 407.

- [49] S. Poeggel, D. Tosi, D. Duraibabu, G. Leen, D. McGrath, E. Lewis, *Sensors* **2015**, *15*, 17115.
- [50] J. D. Huizinga, *Nat. Rev. Gastroenterol. Hepatol.* **2017**, *14*, 372.
- [51] K. M. Sanders, S. M. Ward, G. W. Hennig, *Nat. Rev. Gastroenterol. Hepatol.* **2016**, *13*, 731.
- [52] S. Niu, S. Wang, L. Lin, Y. Liu, Y. S. Zhou, Y. Hu, Z. L. Wang, *Energy Environ. Sci.* **2013**, *6*, 3576.
- [53] C. K. Rayner, M. P. Schwartz, P. S. V. Dam, W. Renooij, M. D. Smet, M. Horowitz, A. J. P. M. Smout, M. Samsom, *Am. J. Gastroenterol.* **2002**, *97*, 3123.
- [54] R. O. Dantas, C. G. Aben-Athar, *Arq. Gastroenterol.* **2002**, *39*, 55.